

## Article

# Prediction and Optimization of Wear Depth on Rectangular Tube Surface in Roll Forming

Menglong Xing <sup>1</sup>, Jiyan Liu <sup>1</sup>, Yuhao Wang <sup>1</sup>, Zhanrui Wang <sup>1</sup>, Yutao Fu <sup>2</sup> and Fengshan Du <sup>1,\*</sup>

<sup>1</sup> National Engineering Research Center for Equipment and Technology of Cold Strip Rolling, Yanshan University, Qinhuangdao 066004, China

<sup>2</sup> Qinhuangdao Chen-Ming Special-Shaped Tube Manufacturing Co., LTD, Qinhuangdao 066000, China

\* Correspondence: fsdu@ysu.edu.cn

**Abstract:** The outer surface of the tube is worn under the interaction between the velocity difference and rolling pressure, in the process of rolling the circular tube into a rectangular tube. In order to predict the wear depth, according to the characteristics of roll forming, the causes of wear in the forming process are analyzed. The finite element model of rolling forming was established based on Archard theory, and the 40 mm × 27.5 mm × 3 mm SUS304 stainless steel rectangular tube was simulated. The simulated results were compared with a test rolling of the steel tubes of the same size material, and the wear areas were found to be highly consistent, which verified the accuracy of the finite element model. The effects of the friction coefficient and the flat roller angular velocity on the simulation results which wear depth were analyzed, and the regression model of wear depth was established by response surface method. The results showed that the flat roller angular velocity had the greatest effect on wear depth; moreover, the flat roller friction coefficient was the second, and the vertical roller friction coefficient was the lowest. The minimum value of the regression model was optimized, the simulation value of the optimization scheme was compared with the optimized value, and the error of the two values was less than 5%, which verified the correctness of the regression model. The wear depth of the rectangular tube after optimization was reduced by 64.69% compared with that before optimization, which verified the effectiveness of the optimization results.



**Citation:** Xing, M.; Liu, J.; Wang, Y.; Wang, Z.; Fu, Y.; Du, F. Prediction and Optimization of Wear Depth on Rectangular Tube Surface in Roll Forming. *Metals* **2023**, *13*, 68. <https://doi.org/10.3390/met13010068>

Academic Editors: Jingwei Zhao, Zhengyi Jiang, Leszek Adam Dobrzański and Chong Soo Lee

Received: 16 November 2022  
Revised: 15 December 2022  
Accepted: 23 December 2022  
Published: 26 December 2022



**Copyright:** © 2022 by the authors. Licensee MDPI, Basel, Switzerland. This article is an open access article distributed under the terms and conditions of the Creative Commons Attribution (CC BY) license (<https://creativecommons.org/licenses/by/4.0/>).

**Keywords:** roll forming; finite element model; tube wear; testing verification; response surface design; optimization

## 1. Introduction

Roll forming plays an important role in plastic processing. Square/rectangular tubing, as one of the most popular forms of cold-formed steel, is widely used in the automobile industry, construction industry, petrochemical industry, and in other fields [1]. According to the forming method, the process can be divided into the direct forming of a square/rectangular tube and a circular tube roll forming a square/rectangular tube. Compared with the direct forming square, the process of a circular tube roll forming a square/rectangular tube has been widely used due to its high forming efficiency and good forming quality. With the continuous development of the manufacturing industry, the requirements for cold-formed products are gradually increasing, especially in the surface quality [2]. Wear, which is considered an important factor, is often observed on the outer surface of the tube, during the forming of the square/rectangular tube, and severely affects the surface quality of the tube.

In the research of plastic forming, the wear problem is mainly reflected in extrusion [3,4], stamping [5,6], rolling [7–9], and so on. Tonn [10] first proposed the formula for calculating abrasive wear in 1937. Archard [11] proposed a wear model for abrasive conditions, which is suitable for the cold extrusion forming [12]. Eriksen [13] studied the influence of die edge geometry on maximum wear and wear distribution in the deep drawing process based

on the finite element model, and verified it through a physical simulation experiment, the results of which showed that the small die curve change could reduce the maximum wear for the actual initial shape. Lee [14] used a non-isothermal ring compression test to estimate the friction coefficient at different temperatures and established the wear coefficient equation through a high-temperature wear test, which has been widely used in wear simulation. Cora [15] studied the wear performance of seven different die samples under the same contact conditions, and the results showed that D2's surface scratches were clearly visible. The mass loss of 0050A cast steel is the highest; however, no galling effect was observed on the contact surface. The wear pattern is almost uniform along the contact surface for the sample of Vancron 40; Vanadis 4 extra, K340 Isodur, and Carmo had similar wear rate values. Pereira [16] adopted a novel technique to study the influence of the die corner radius shape on the wear behavior during sheet metal stamping, and the results showed that the small changes of the die radius profile shape can result in seriously reduced tool life, and that this phenomenon could be explained based on numerical simulation. Li T.T. [17] and Zhang C.S. [18] conducted the cold extrusion of an aluminum tube to study the influence of process parameters on die wear depth, which provides useful guidance for predicting die life. Xu W.J [19] proposed a new calculation model based on the wear of the die, optimized the geometric structure of the die, and verified the accuracy of the model through the wear test. Hawryluk [20], through their research of the wear of a punch used in cover-type forging, proved that there are different wear mechanisms in the specific areas of the tools; moreover, the research results have shown that finite element analysis based on the Archard model is inadequate in areas where many failure mechanisms occur simultaneously. Farzad [21] proposed a new incremental slab method to calculate the extrusion pressure distribution and the wear depth, and the results showed that the extrusion load and die pressure distribution predicted by the method are in good agreement with the finite element results, and that the proposed method has a promising application prospect. Ogbezode [22] embedded the wear model subroutine into the finite element to calculate the die wear depth during the extrusion process of C-shaped Equal Channel Reciprocating Extrusion (CECRE) die of magnesium alloy, the results of which showed that the die wear depth reached the maximum under the conditions of the lowest friction coefficient, and that the wear area was mainly concentrated on the shear planes of die components, leading to a less ductile CECRE product. Davoudi [23] used the DEFORM finite element model code to predict the wear behavior of the hot forging die and obtained the key wear points on the die surface, based on Taguchi method, allowing an empirical model for predicting the wear of hot forging die to be established, which provided a reference for die design and the hot forging industry.

Based on the above research, most scholars' research has mainly reflected the wear of the die; however, the wear of the deformable body is relatively less, especially in the field of roll forming. Compared with the direct forming of rectangular tubes, greater force is required when the circular tube roll is forming rectangular tubes, which is conducive to the occurrence of tube surface wear. When the circular tube roll is forming a rectangular tube, the relative sliding velocity in the side area of the rectangular tube is large due to the pass shape, which makes the area prone to scratch phenomenon, leading to a reduction in the quality of the product.

In order to reduce the surface wear of the rectangular tube and improve the product quality effectively in actual production, this work studied the surface wear of rectangular tubes by means of finite element simulation and testing verification, explored the influence of forming process parameters on the wear, and optimized it based on the regression model. The finite element model provides guidance for the actual production.

## 2. Analysis of Rectangular Tube Forming

### 2.1. Principle of Roll Forming

The process of the circular tube roll forming square/rectangular tube is shown in Figure 1.

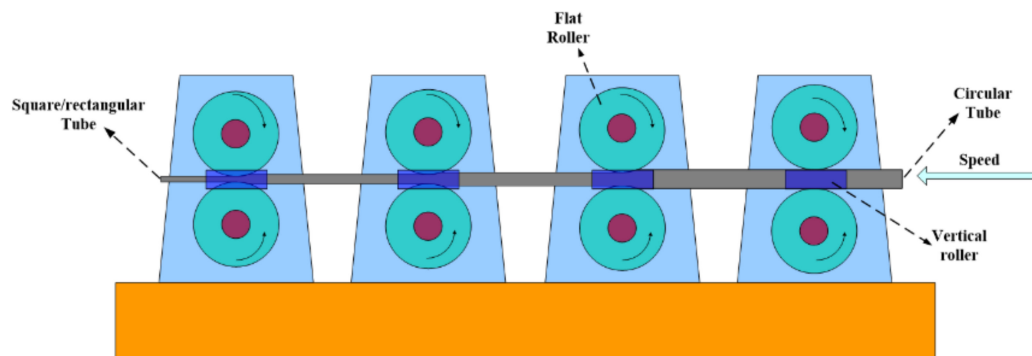


**Figure 1.** Diagram of a circular tube roll forming a rectangular tube.

In roll forming, the law of constant volume and the principle of equal metal flow per second should be satisfied [24]:

$$\begin{cases} C_{M-1(NL)} = k_M \cdot C_{M(NL)} = \mu_M \cdot \varepsilon_M \cdot C_{M(NL)} \\ \frac{R_M}{R_{M-1}} = \mu'_M \end{cases} \quad (1)$$

where  $C_{M-1(NL)}$  is the circumference of the neutral layer on the  $(M - 1)$ -th pass.  $k_M$  is the  $(M)$ -th pass expansion coefficient.  $C_{M(NL)}$  is the circumference of the neutral layer on the  $(M)$ -th pass.  $\mu_M$  is the  $(M)$ -th pass elongation coefficient.  $\varepsilon_M$  is the thickening coefficient of the  $(M)$ -th pass.  $R_M$  is the average roller radius of the  $(M)$ -th pass.  $R_{M-1}$  is the average roller radius of the  $(M - 1)$ -th pass.  $\mu'_M$  is the average extension coefficient of the  $(M)$ -th pass.

In theory,  $\mu_M = \mu'_M = \text{constant}$ . Due to the effect of the pass shape, the particle on the tube has a certain difference on the axial velocity, and a floating interval will appear on  $\mu'_M$ . When the difference between the overall tube velocity and the particle velocity is large, the possibility of the tube surface wear will be increased.

## 2.2. Force Analysis of Particles on the Tube

In order to avoid the difficulty of roll forming, the deformation difference between passes should be reduced, and the bite condition is (Figure 2) [25,26]:

$$\begin{aligned} T_x &> N_x + N'_x + T'_x \\ T_x &= T \cos \theta \\ N_x &= N \sin \theta \\ N'_x &= N' \sin \theta' \\ T'_x &= T' \cos \theta' \end{aligned} \quad (2)$$

where  $T_x$  is the horizontal component of the friction force on flat roller.  $N_x$  is the horizontal component of the normal force on flat roller.  $N'_x$  is the horizontal component of the normal force on vertical roller.  $T'_x$  is the horizontal component of the friction force on vertical roller.  $T$  is the friction force of flat roller.  $\theta$  is the bite Angle of flat roller.  $N$  is the normal force of flat roller.  $N'$  is the normal force of vertical roller.  $\theta'$  is the bite Angle of vertical roller.  $T'$  is the friction force of vertical roller.

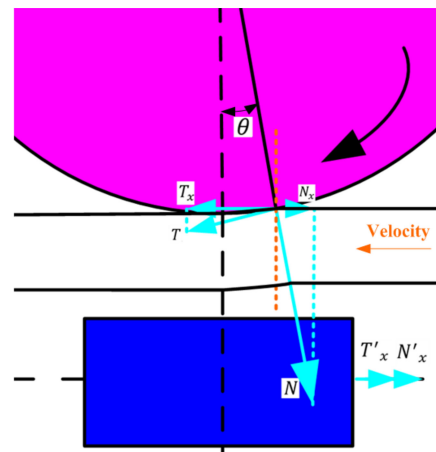


Figure 2. Diagram of the bite condition.

The force analysis of the particles in the middle region and edge region on the rectangular tube is carried out (Figure 3). In the Z direction, the difference between the velocity values of particle 2 and the tube is greater than that of particle 1 and the tube. In the Y direction, the contact normal force on particle 2 is greater than that on particle 1. The wear at particle 2 is likely to be the most severe, comparing the two influencing factors of contact normal stress and relative sliding velocity.

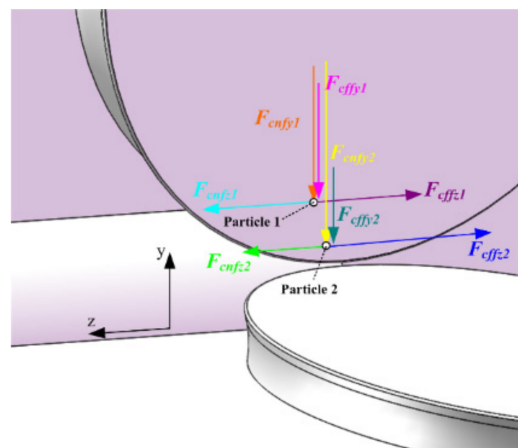


Figure 3. Force analysis of particles.

### 3. Finite Element Model

#### 3.1. Flow Stress Model

Uniaxial tensile test is carried out on an SUS304 stainless steel sample. The chemical compositions of SUS304 stainless steel are shown in Table 1. The tensile speed is 3 mm/min, the standard distance length is 50 mm, and the thickness of the sample is 3 mm. The flow stress model is fitted using the piecewise fitting method, which is not effective due to direct fitting [27]. The equation is:

$$\begin{cases} \sigma_0 = E \cdot \epsilon_e \\ \sigma_1 = \sigma_s + A_1 \epsilon_p^{n1} (0 \leq \epsilon_p < 0.02) \\ \sigma_2 = A_2 \epsilon_p^{n2} \cdot \exp(b \epsilon_p) (\epsilon_p \geq 0.02) \end{cases} \quad (3)$$

where  $\sigma_i$  is the flow stress ( $i = 0, 1, 2$ );  $\sigma_s$  is the yield stress;  $\epsilon_p$  is the equivalent plastic strain;  $E$  is the elastic modulus;  $\epsilon_e$  is the elastic strain;  $A_1, A_2, n1, n2$ , and  $b$  are the material parameters. In the flow stress model fitting, the curve continuity condition should be

satisfied at  $\varepsilon_p = 0.02$  (Figure 4), and the results of the relevant parameters are shown in Table 2.  $A_1$ ,  $n_1$ ,  $A_2$ ,  $n_2$ , and  $b$  are calculated as follows

$$\begin{cases} \sigma_1 = \sigma_s + A_1 \varepsilon_p^{n_1} (0 \leq \varepsilon_p < 0.02) \\ \varepsilon_p = 0.01, \sigma = 345.41 \\ \varepsilon_p = 0.02, \sigma = 375 \end{cases} \quad (4)$$

$$\begin{cases} \sigma_2 = A_2 \varepsilon_p^{n_2} \cdot \exp(b \varepsilon_p) (\varepsilon_p \geq 0.02) \\ \sigma'_1 = \sigma'_2 (\varepsilon_p = 0.02) \\ \varepsilon_p = 0.02, \sigma = 375 \\ \varepsilon_p = 0.23, \sigma = 760.15 \end{cases} \quad (5)$$

**Table 1.** Chemical compositions (wt%) of SUS304 stainless steel.

C	Si	Mn	P	S	Ni	Cr
≤0.08	≤1	≤2	≤0.045	≤0.03	8~10.5	18~20

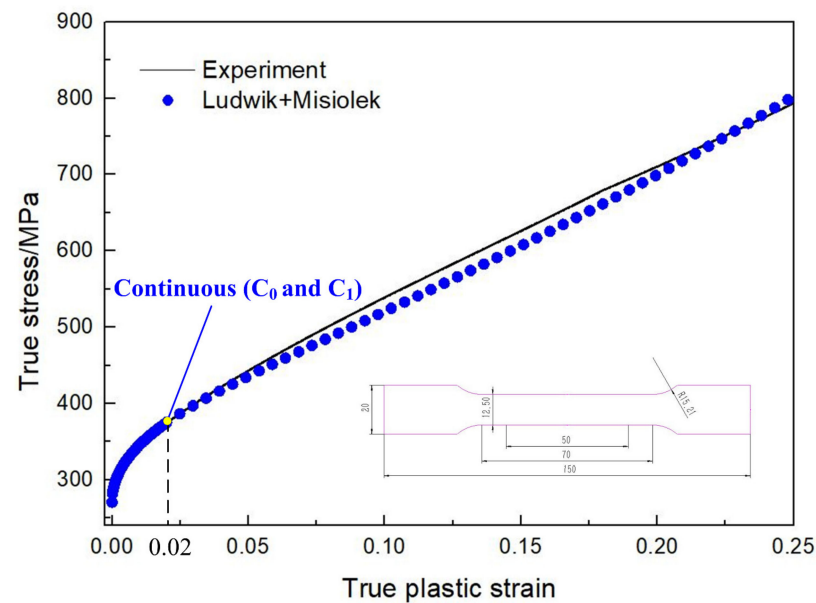


**Figure 4.** Fitting result of the flow stress model.

**Table 2.** SUS304 stainless steel material parameters.

Parameters	$E$ (MPa)	$\sigma_s$ (MPa)	$H$ (HV)	$K$	$A_1$	$n_1$	$A_2$	$n_2$	$b$
values	199,046	270.61	200	$2.985 \times 10^{-6}$	684.93	0.48	502.26	0.087	2.36

### 3.2. Calculation Model of Wear Depth

Based on the Archard wear model, the wear rate at the contact point is [11]

$$\dot{w} = \frac{K}{H} \cdot \sigma_n \cdot V_{re} \quad (6)$$

where  $\dot{w}$  is the wear rate (mm/s).  $K$  is the wear coefficient, the value ranges from  $10^{-7} \sim 10^{-2}$  [21,28].  $H$  is the material hardness (HV).  $\sigma_n$  is the contact normal stress (MPa);  $V_{re}$  is the relative sliding velocity of the contact surface (mm/s). The specific parameters are shown in Table 2.

In finite element calculation, the cumulative wear depth is represented by the wear index

$$w_{n+1} = w_n + \dot{w} \cdot \Delta t \quad (7)$$

where  $w_{n+1}$  is the wear depth of step  $n + 1$  (mm).  $w_n$  is the wear depth of step  $n$ ;  $\dot{w}$  is the increment of time (s).

### 3.3. Simulation Model

The finite element model of the small corner SUS304 stainless steel rectangular tube ( $40 \text{ mm} \times 27.5 \text{ mm} \times 3 \text{ mm}$ ) was established in MSC.MARC (Figure 5). The flow stress model is written in the FORTRAN language based on a WKSLP subroutine. The Archard model can be set up in MENTAT or written in the FORTRAN language based on the UWEARINDEX subroutine. The wear depth is calculated during the contact between the roller and the tube. The accumulated wear depth is displayed using custom nodes. A 1/4 model, for which rectangular tube forming is symmetrical, was established to reduce the computation. There is a total of five passes in the forming process: the first pass is the sizing stage, and the model is established from the second pass. The roller is defined as a rigid body, while the tube is defined as a deformable body. Two symmetrical planes are set in the X and Y directions. The tube is divided by hexahedral mesh, and the mesh is subdivided in the corner area. At the entrance, the tube is pushed into the pass through the push plate; after the roll forming is stable, the push plate is cancelled. According to the principle of equal metal flow per second, the push plate velocity should be less than the linear velocity of the flat roller at the entry pass. In the forming process, the flat roller is the driven roller, and the vertical roller is the idler roller. The roller diameter increases gradually with an increase in pass. According to Formula (2), the vertical roller is kept in a smooth state in the actual production process, therefore the friction resistance of the vertical roller is ignored, and the friction coefficient of the flat roller should conform to the formula

$$\begin{cases} T'_x \approx 0 \\ T_x > N_x + N'_x \\ N'_x = K \cdot N_x \\ \mu > (1 + K) \tan \theta \end{cases} \quad (8)$$

where  $K$  is the proportional coefficient;  $\mu$  is the friction coefficient of the flat roller.

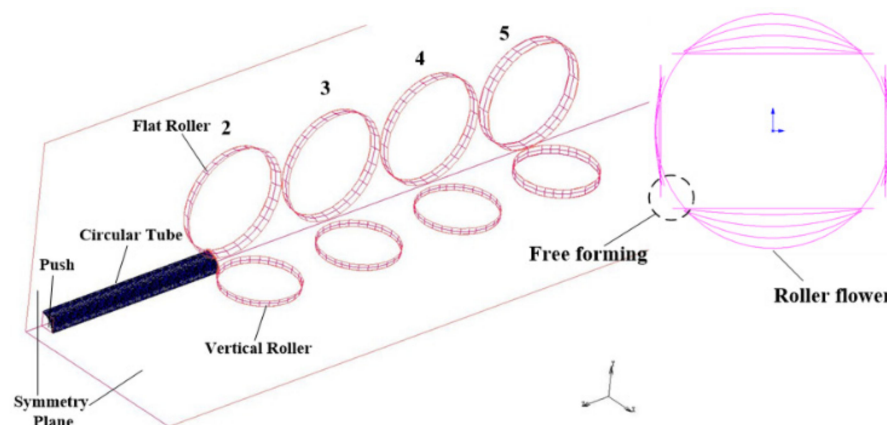


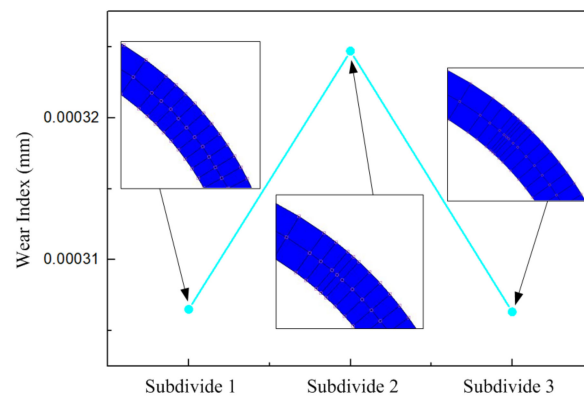
Figure 5. Simulation model of roll forming.

Combined with Equation (8) and references [25,29,30], the friction coefficient of the flat roller was set as 0.2 (Table 3). Because the vertical roller rotates freely, the friction coefficient was set as 0.001 [25].

**Table 3.** Roll forming parameters.

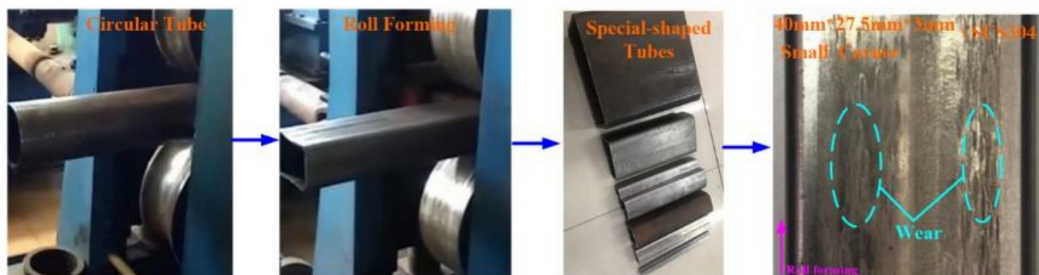
Parameters	Friction Coefficient of Flat Roller	Friction Coefficient of Vertical Roller	Flat Roller Angular Velocity	Diameter of the Circular Tube	Thickness of the Circular Tube	Diameter of the Second Pass at the Top of the Flat Roller	Flat Roller Diameter of the 5th Pass
values	0.2	0.001	2 rad/s	47 mm	3 mm	158 mm	164 mm

The simulation results based on grid independence verification (Figure 6) show that the node wear depth has little change with an increase in corner mesh. The mesh division was reasonable, and an increase in the mesh is not sensitive to the forming results.

**Figure 6.** Grid independence verification.

### 3.4. Testing Verification

Figure 7 shows the test process of the rectangular tube roll forming. It is found that there is significant surface wear in the side area of the rectangular tube, which is consistent with the analysis in Section 2.2.

**Figure 7.** Roll forming test.

By comparing the simulation results with the test (Figure 8a,b), it can be seen that the simulation results of the section size are in good agreement with the test, which verifies the accuracy of the finite element model. Under an FEI-SCIOS scanning electron microscope (FEI, Hillsboro, OR, USA), the wear areas on the surface were observed using a scanning voltage of 10 kV and a current of 0.4 nA (Figure 8e,f). There are some defects on the worn surface, such as plastic deformation, grooves, material spalling pits, and tiny wear chips; moreover, the wear in the forming process is mainly adhesive wear and particle wear. The wear area on the surface of the rectangular tube was compared with the simulation results (Figure 8c,d), and it can be seen that the test and simulation have a high coincidence, which verifies the feasibility of the wear model.

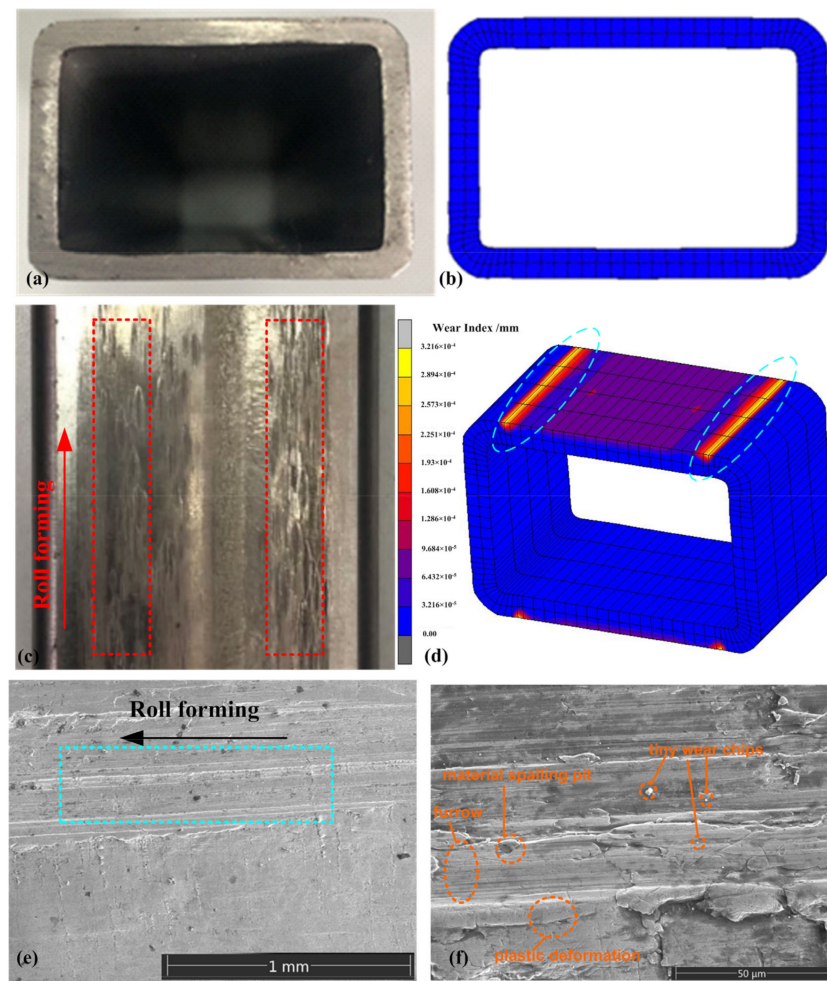


**Figure 8.** The test results are compared with the simulation results: (a) Dimension of the section forming. (b) Simulation of the section forming. (c) Wear on the surface of the rectangular tube. (d) wear simulation. (e) Scanning electron microscope (SEM) photo of the wear area. (f) SEM photo of the area enlargement.

#### 4. Prediction and Optimization of Rectangular Tube Surface Wear

##### 4.1. Influences of Process Parameters on Surface Wear

The effect of the flat roller angular velocity on the wear depth was analyzed by finite element simulation results (Figure 9). When the flat roller angular velocity increased, the wear depth also increased gradually. As can be seen from Figure 10, with an increase in the angular velocity, the relative sliding velocity and contact normal stress in the wear area increase, resulting in an increase in wear rate. Therefore, in the actual production process, on the premise of ensuring the production efficiency, the forming velocity should be lower, which can reduce the relative sliding velocity and wear depth.

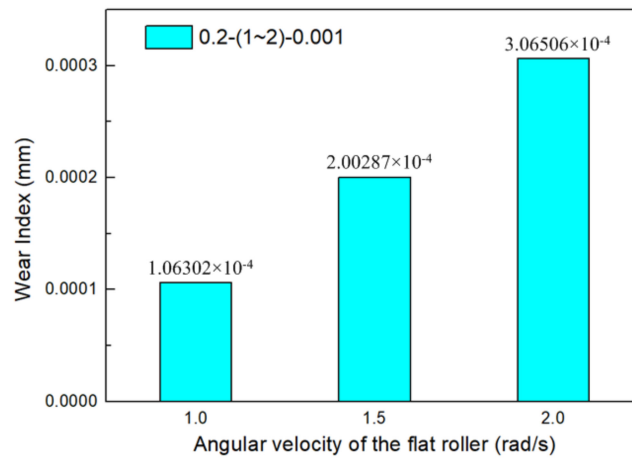


Figure 9. Influence of flat roller angular velocity on wear depth.

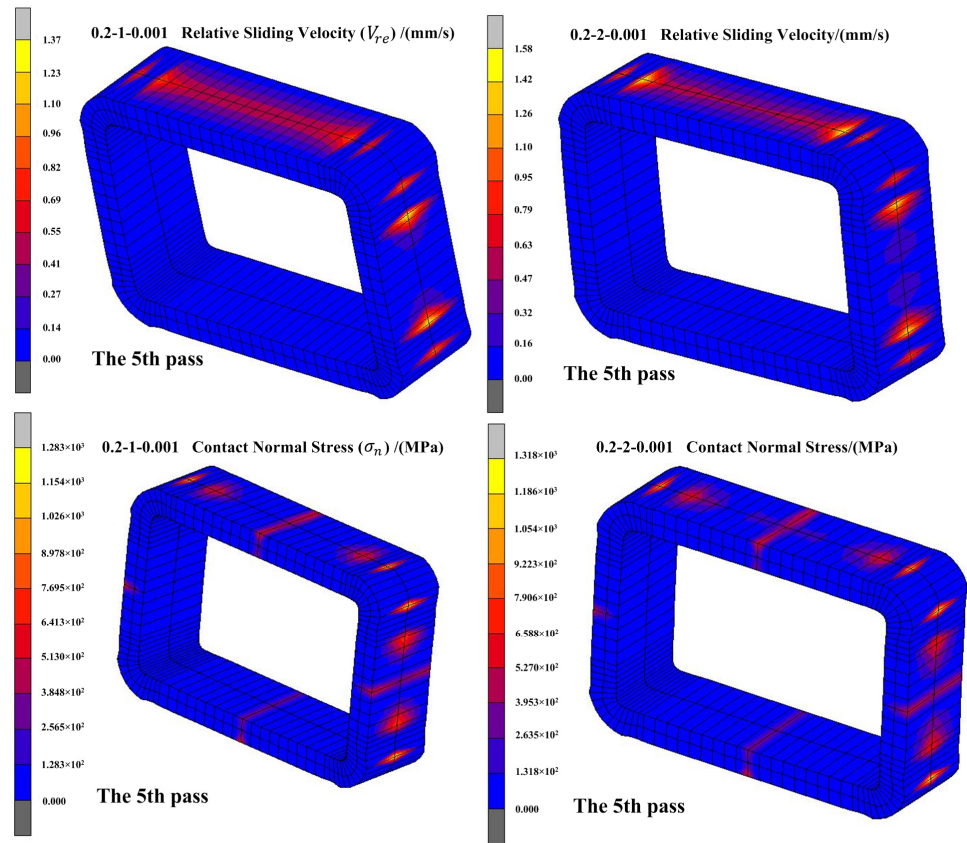


Figure 10. Simulation results of wear parameters under different flat roller angular velocity.

In the finite element model, the surface wear was analyzed by changing the friction coefficient between the flat roller and the tube (Figure 11), and it can be clearly observed that, with an increase in the friction coefficient, the wear depth first decreases and then increases; however, the trend change is not obvious. Combined with Figure 12, the relative sliding velocity and contact normal stress of the two schemes are almost unchanged, and the wear depth tends to be consistent.

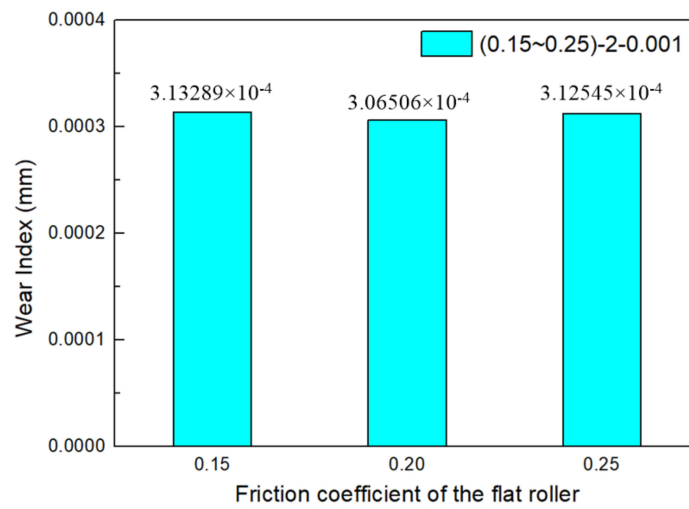


Figure 11. Influence of flat roller friction coefficient on wear depth.

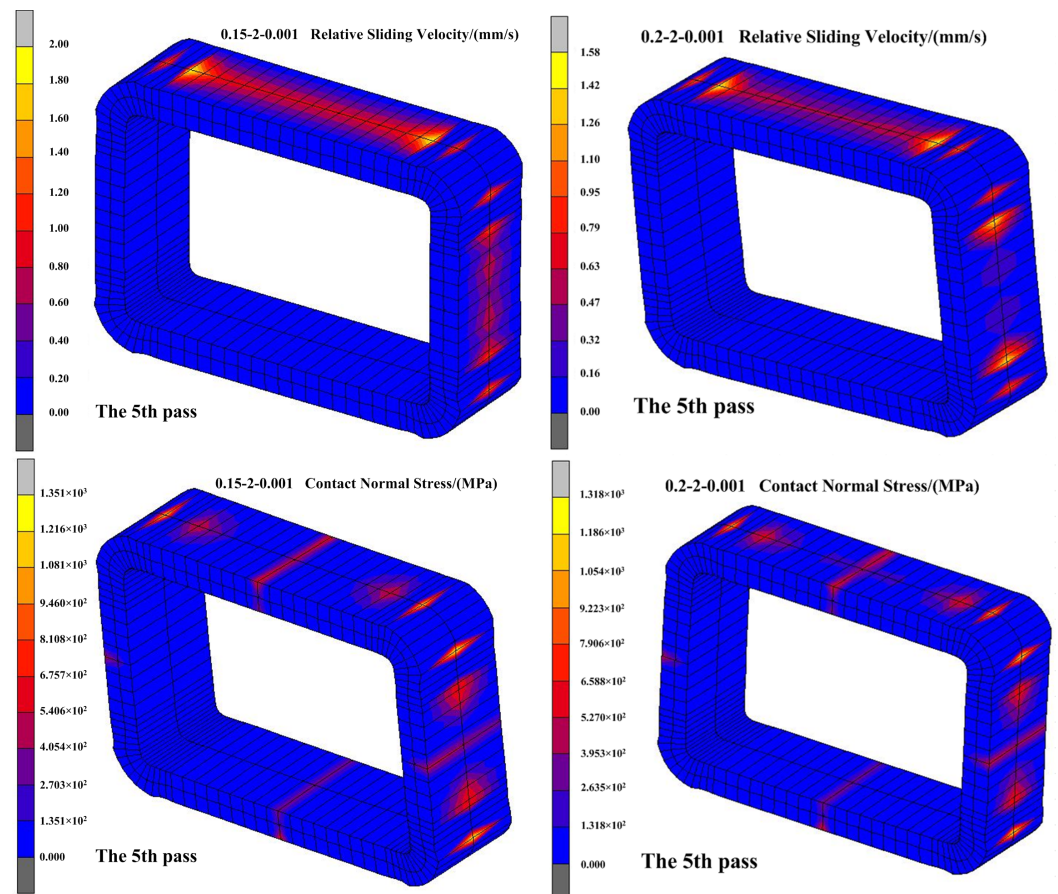


Figure 12. Simulation results of wear parameters under different flat roller friction coefficient.

The influence of the vertical roller friction coefficient on the wear depth was analyzed (Figure 13). It can be seen that, with an increase in the friction coefficient, the wear depth first decreases and then increases. Figure 14 shows that, when the friction coefficient is 0.01, the relative sliding velocity is higher and the contact normal stress does not change significantly, which results in a higher wear rate and a relatively large wear depth.

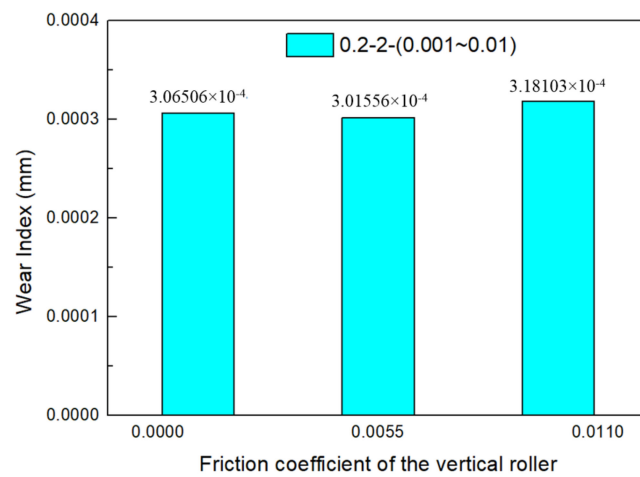


Figure 13. Influence of vertical roller friction coefficient on wear depth.

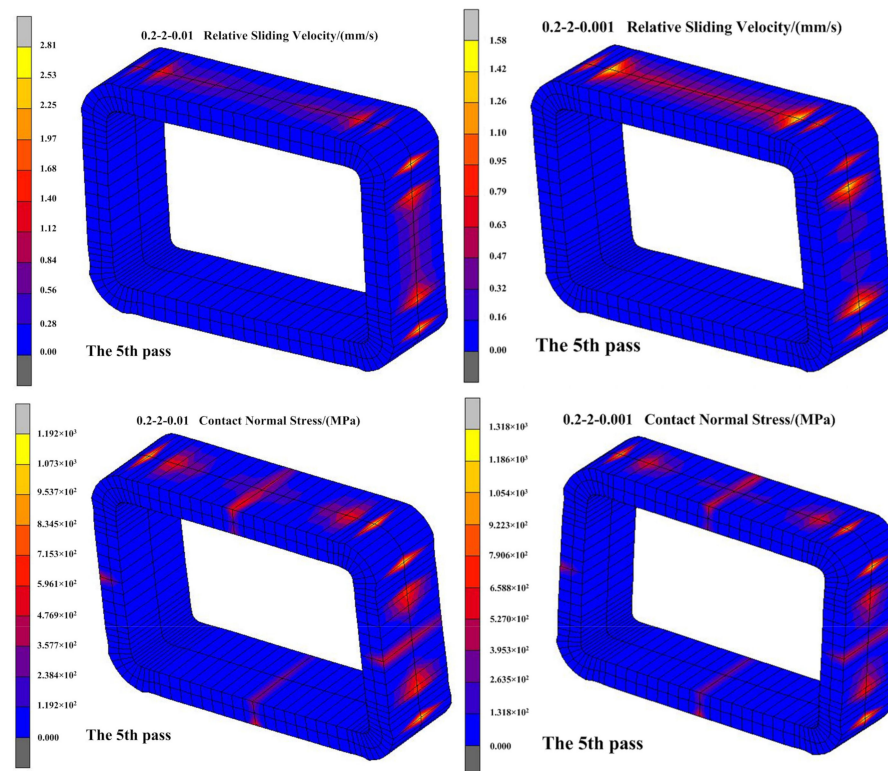


Figure 14. Simulation results of wear parameters under different vertical roller friction coefficient.

#### 4.2. Prediction Model and Variance Analysis of Wear Depth

Box–Behnken Design (BBD) is a frequently used test design method in response to surface analysis, and it has been widely used because of its low test times and high efficiency [31,32]. The process parameters in Section 4.1 were taken as impact factors, and the BBD was carried out using a simulation instead of a test. The wear depth of the same node in the wear area was taken as the response value. The specific calculation results are shown in Table 4.

**Table 4.** BBD and results.

Process No.	A	B	C	Wear Index (mm)
1	0.15	1.5	0.01	0.000207997
2	0.2	2	0.001	0.000306506
3	0.2	1.5	0.0055	0.000200535
4	0.25	1.5	0.01	0.000194054
5	0.15	1.5	0.001	0.000217845
6	0.2	1.5	0.0055	0.000200535
7	0.2	1.5	0.0055	0.000200535
8	0.15	2	0.0055	0.000304261
9	0.2	1	0.01	0.000125557
10	0.25	2	0.0055	0.000293714
11	0.25	1	0.0055	0.000127219
12	0.25	1.5	0.001	0.000200883
13	0.15	1	0.0055	0.000109441
14	0.2	1	0.001	0.000106302
15	0.2	2	0.01	0.000318103
16	0.2	1.5	0.0055	0.000200535
17	0.2	1.5	0.0055	0.000200535

The regression model of wear depth is

$$Y = -0.0000829967 + 0.000411121A + 0.00014757B - 0.0017489C - 0.00028325AB + 0.00335444AC - 0.000850889BC - 0.0001597A^2 + 0.000034092B^2 + 0.24983C^2 \quad (9)$$

where  $Y$  is the wear depth.  $A$  is the flat roller friction coefficient.  $B$  is the flat roller angular velocity.  $C$  is the vertical roller friction coefficient. The variance analysis of the model is shown in Table 5. It can be seen that the model has a significant impact on the response value due to the  $P$  value of the model being less than 0.05.  $R^2 = 0.9919$  approaches 1, indicating that the model has a high degree of fitting, and that the regression model can reflect the relationship between factors and responses. The SNR is 28.841, which is greater than 4 and within the reasonable range. The order of the influencing factors of wear depth is as follows:  $B > A > C$ . Figure 15a shows the fitting results of the simulated value and predicted value. The error of the two values is small, indicating that the prediction ability of the model is effective. Based on the above analysis, it can be shown that the virtual simulation data can be used to establish the regression model. The wear depth gradually increases with an increase in flat roller angular velocity, and the friction coefficient has no significant effect on the wear depth (Figure 15b). The interaction between  $A$  and  $B$  is relatively obvious, and the wear depth is maximum in the area of low  $A$  and high  $B$ . The interaction between  $A$  and  $C$  is not obvious, and the same applies to  $B$  and  $C$  (Figure 15c).

**Table 5.** Variance analysis of wear depth regression model.

Source	SS	DF	MS	F-Value	$p$ -Value	
Model	$7.182 \times 10^{-8}$	9	$7.980 \times 10^{-9}$	95.06	<0.0001	significant
A	$7.006 \times 10^{-11}$	1	$7.006 \times 10^{-11}$	0.83	0.3914	
B	$7.108 \times 10^{-8}$	1	$7.108 \times 10^{-8}$	846.6	<0.0001	
C	$2.512 \times 10^{-11}$	1	$2.512 \times 10^{-11}$	0.3	0.6014	
AB	$2.006 \times 10^{-10}$	1	$2.006 \times 10^{-10}$	2.39	0.1661	
AC	$2.279 \times 10^{-12}$	1	$2.279 \times 10^{-12}$	0.027	0.8738	
BC	$1.466 \times 10^{-11}$	1	$1.466 \times 10^{-11}$	0.17	0.6885	
$A^2$	$6.712 \times 10^{-13}$	1	$6.712 \times 10^{-13}$	$7.994 \times 10^{-3}$	0.9313	
$B^2$	$3.059 \times 10^{-10}$	1	$3.059 \times 10^{-10}$	3.64	0.0979	
$C^2$	$1.078 \times 10^{-10}$	1	$1.078 \times 10^{-10}$	1.28	0.2945	
Residual	$5.877 \times 10^{-10}$	7	$8.396 \times 10^{-11}$			
Lack of fit	$5.877 \times 10^{-10}$	3	$1.959 \times 10^{-10}$			
Pure Error	0.000	4	0.000			
Cor Total	$7.241 \times 10^{-8}$	16				

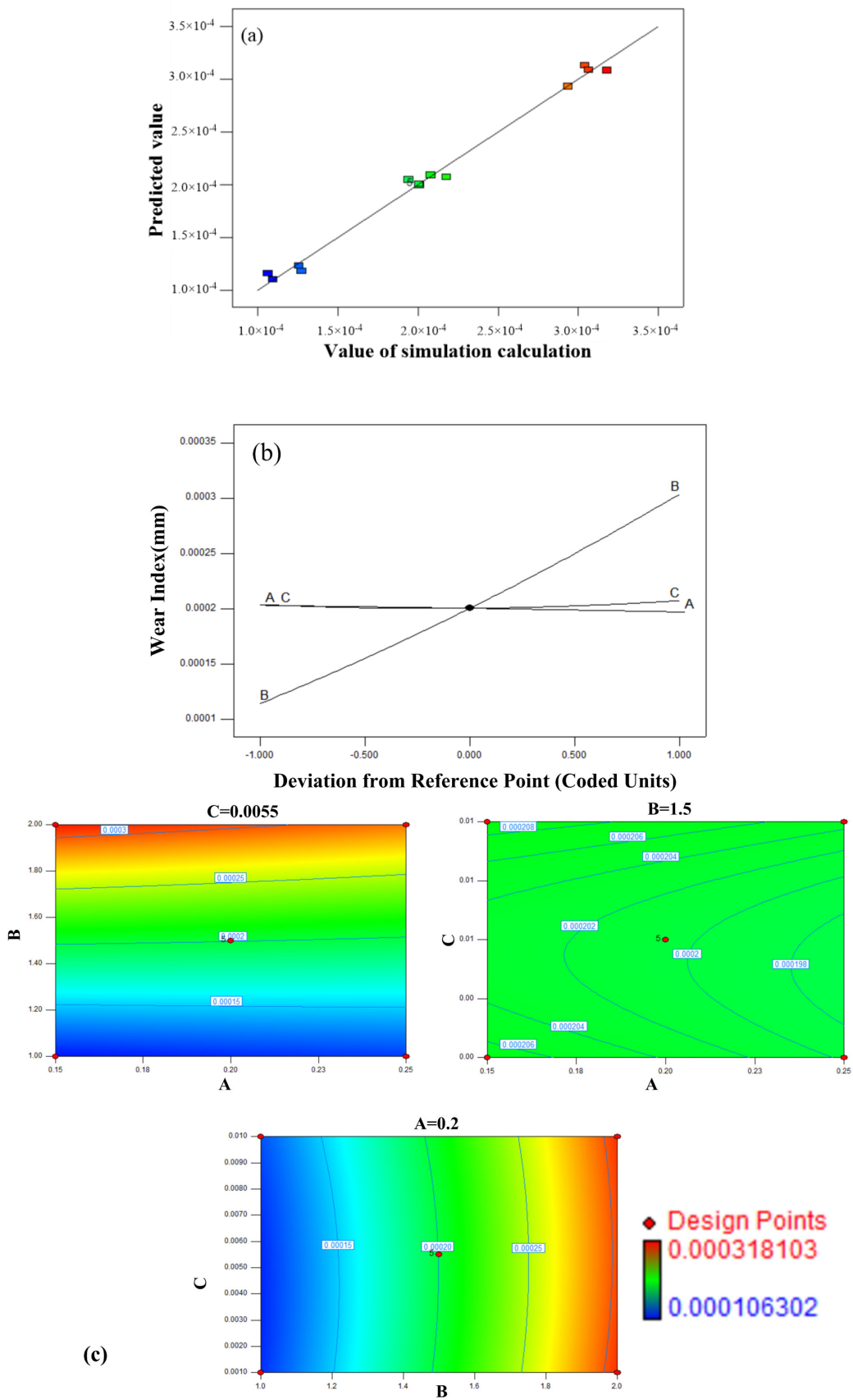


Figure 15. Influence curve of wear depth: (a) The fitting of predicted and simulated values. (b) Single factor perturbation curve. (c) Contour of the interaction on influence factors.

### 4.3. Optimization of the Regression Model

In order to reduce the wear depth of the rectangular tube surface, minimum optimization of regression model was carried out, and the problem was described as follows:

$$\begin{cases} f = \min(Y) \\ s.t. \quad 1 \leq B \leq 2 \\ \quad 0.001 \leq C \leq 0.1 \\ \quad 0.15 \leq A \leq 0.25 \end{cases} \quad (10)$$

The optimization results are shown in Figure 16. The selected optimization scheme is  $A = 0.15$ ,  $B = 1$  rad/s,  $C = 0.0042$ , and the optimization value of the regression model is 0.0001099 mm. The simulation wear depth of the optimization scheme is 0.000108248 mm, compared with the optimization value of the regression model, the error of the two is less than 5%, which verifies the accuracy of the regression model. The simulation results of the optimization scheme are compared with the original simulation results (Figure 17), and the wear depth is reduced by 64.69%, which verifies the effectiveness of the optimization scheme. The flow chart of the article is shown in Figure 18.

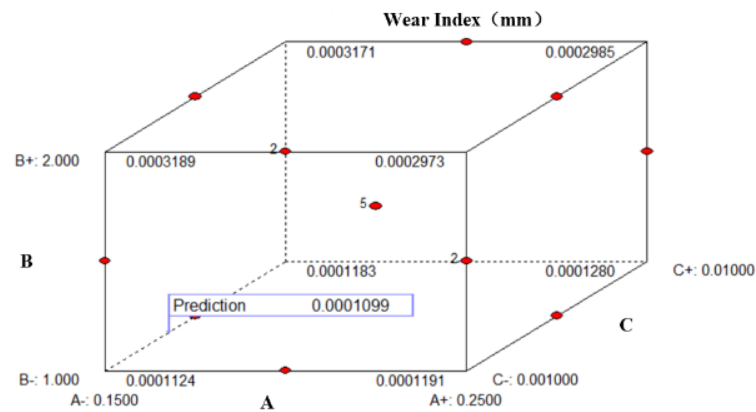


Figure 16. Optimization results of the regression model.

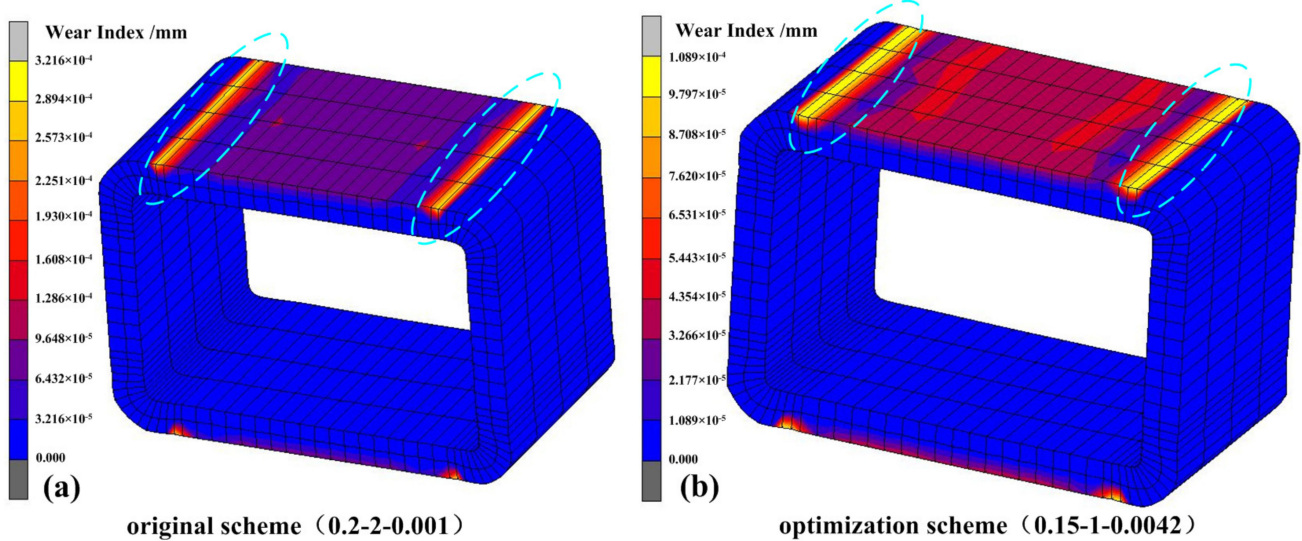
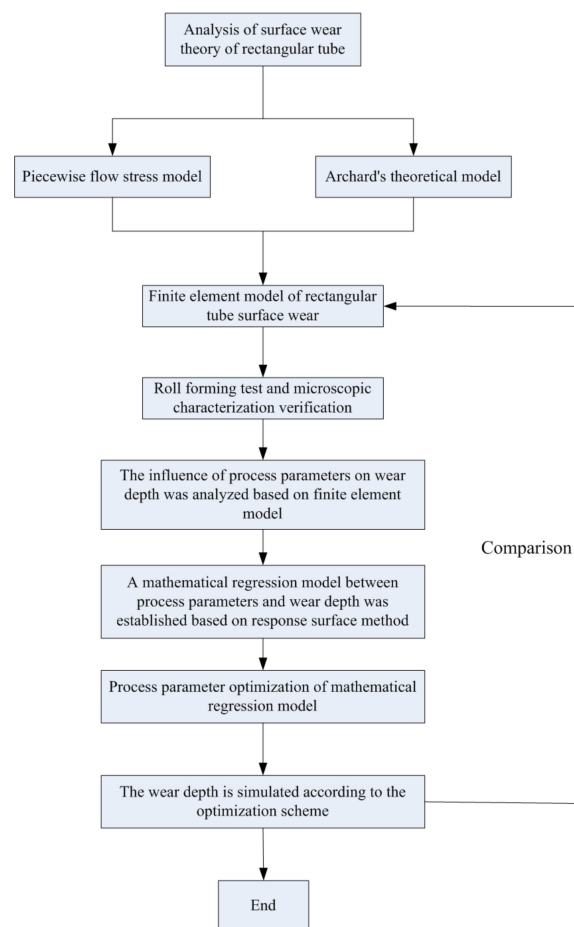


Figure 17. Simulation comparison of wear depth: (a) original scheme; (b) optimization scheme.



**Figure 18.** Flow chart of the wear analysis.

## 5. Conclusions

(1) According to the characteristics of a circular tube roll forming a rectangular tube, the possible wear area was analyzed. The finite element model of roll forming was established based on Archard theory, and the roll forming test was carried out. The simulation results were compared with the test, and the section size and wear area of the two were in good agreement, which verified the accuracy of the simulation model.

(2) The effects of the friction coefficient and flat roller angular velocity on wear depth were analyzed, and a regression model of the wear depth was established based on the response surface method. Through variance analysis, it is found that the flat roller angular velocity has the greatest influence, followed by the flat roller friction coefficient, and that the vertical roller friction coefficient is the least. The regression model can predict the wear depth.

(3) The minimum value of the regression model was optimized, and the simulation results of the optimization scheme were compared with the optimized value; moreover, the error between the two was less than 5%, which verified the accuracy of the regression model. By comparing the simulation results of the optimization scheme with the original scheme, the wear depth is reduced by 64.69%, which verified the effectiveness of the optimization scheme.

**Author Contributions:** Data curation, M.X. and J.L.; Methodology, F.D.; Project administration, F.D.; Software, M.X. and Z.W.; Validation, M.X., Y.W. and Y.F.; Writing—original draft, M.X. All authors have read and agreed to the published version of the manuscript.

**Funding:** The authors would like to thank the support from the National Natural Science Foundation of China (51975510) and the Natural Science Foundation of HeBei Province (E2017203043).

**Conflicts of Interest:** The authors declare that they have no conflict of interest.

## References

1. Hiroshi, O.; Liu, J.Y. *Cold Roll Forming Technology*; Chemical Industry Press: Beijing, China, 2008. (In Chinese)
2. Halmos, G.T. *Roll Forming Handbook*; Chemical Industry Press: Beijing, China, 2006. (In Chinese)
3. Wang, Y.J.; Jia, Z.; Ji, J.J.; Wei, B.; Heng, Y.; Liu, D. Determining the wear behavior of H13 steel die during the extrusion process of pure nickel. *Eng. Fail. Anal.* **2022**, *134*, 106053. [[CrossRef](#)]
4. Kumar, P.; Joshi, R.S.; Singla, R.K. Sliding wear behaviour of CP titanium laminates produced by large strain extrusion machining. *Wear* **2021**, *477*, 203774. [[CrossRef](#)]
5. Bang, J.; Kim, M.; Bae, G.; Song, J.; Kim, H.-G.; Lee, M.-G. Quantitative Evaluation of Tool Wear in Cold Stamping of Ultra-High-Strength Steel Sheets. *Met. Mater. Int.* **2022**. [[CrossRef](#)]
6. Bang, J.; Kim, M.; Bae, G.; Kim, H.-G.; Lee, M.-G.; Song, J. Efficient Wear Simulation Methodology for Predicting Nonlinear Wear Behavior of Tools in Sheet Metal Forming. *Materials*. **2022**, *15*, 4509. [[CrossRef](#)]
7. Peng, Z.S.; Ji, H.C.; Huang, X.M.; Wang, B.Y.; Xiao, W.C.; Wang, S.F. Numerical analysis and parameter optimization of wear characteristics of titanium alloy cross wedge rolling die. *Metals* **2021**, *11*, 1998. [[CrossRef](#)]
8. Ji, H.C.; Song, G.; Song, C.Z.; Li, J.S.; Pei, W.C.; Wang, B.Y. Analysis of the wear characteristics of multi-directional die forging and forming dies for a railway wagon bogie adapter. *Int. J. Adv. Manuf. Technol.* **2022**, *123*, 2351–2370. [[CrossRef](#)]
9. Huang, H.; Chen, X.; Fan, B.; Jin, Y.; Shu, X. Initial billet temperature influence and location investigation on tool wear in cross wedge rolling. *Int. J. Adv. Manuf. Technol.* **2015**, *79*, 1545–1556. [[CrossRef](#)]
10. Kragelsky, I.V.; Dobychin, M.N.; Kombatov, V.S. *Friction and Wear: Calculation Methods*; Elsevier: Amsterdam, The Netherlands, 2013.
11. Archard, J. Contact and rubbing of flat surfaces. *J. Appl. Phys.* **1953**, *24*, 981–988. [[CrossRef](#)]
12. Sobis, T.; Engel, U.; Geiger, M. A theoretical study on wear simulation in metal forming processes. *J. Mater. Process. Technol.* **1992**, *34*, 233–240. [[CrossRef](#)]
13. Eriksen, M. The influence of die geometry on tool wear in deep drawing. *Wear* **1997**, *207*, 10–15. [[CrossRef](#)]
14. Lee, R.S.; Jou, J.L. Application of numerical simulation for wear analysis of warm forging die. *J. Mater. Process Technol.* **2003**, *140*, 43–48. [[CrossRef](#)]
15. Cora, O.N.; Koc, M. Experimental investigations on wear resistance characteristics of alternative die materials for stamping of advanced high-strength steels (AHSS). *Int. J. Mach. Tools Manuf.* **2009**, *49*, 897–905. [[CrossRef](#)]
16. Pereira, M.P.; Weiss, M.; Rolfe, B.F.; Hilditch, T.B. The effect of the die radius profile accuracy on wear in sheet metal stamping. *Int. J. Mach. Tools Manuf.* **2013**, *66*, 44–53. [[CrossRef](#)]
17. Li, T.T.; Zhao, G.Q.; Zhang, C.S.; Guan, Y.J.; Sun, X.M.; Li, H.K. Effect of process parameters on die wear behavior of aluminum alloy rod extrusion. *Mater Manuf Processes*. **2013**, *28*, 312–318. [[CrossRef](#)]
18. Zhang, C.S.; Zhao, G.Q.; Li, T.T.; Guan, Y.J.; Chen, H.; Li, P. An investigation of die wear behavior during aluminum alloy 7075 tube extrusion. *J. Tribol. T Asme*. **2013**, *135*, 011602. [[CrossRef](#)]
19. Xu, W.J.; Li, W.H.; Wang, Y.S. Experimental and theoretical analysis of wear mechanism in hot-forging die and optimal design of die geometry. *Wear* **2014**, *318*, 78–88. [[CrossRef](#)]
20. Hawryluk, M.; Kaszuba, M.; Gronostajski, Z.; Polak, S.; Ziemia, J. Identification of the relations between the process conditions and the forging tool wear by combined experimental and numerical investigations. *CIRP J. Manuf. Sci. Technol.* **2020**, *30*, 87–93. [[CrossRef](#)]
21. Farzad, H.; Ebrahimi, R. An investigation of die profile effect on die wear of plane strain extrusion using incremental slab method and finite element analysis. *Int. J. Adv. Manuf. Technol.* **2020**, *111*, 627–644. [[CrossRef](#)]
22. Ogbezode, J.E.; Ajide, O.O. Tool wear analysis of C-shaped equal channel reciprocating extrusion process of AISI-H13 steel die using finite element method. *J. Braz. Soc. Mech. Sci.* **2021**, *43*, 568. [[CrossRef](#)]
23. Davoudi, M.; Nejad, A.F.; Koloor, S.S.R.; Petrù, M. Investigation of effective geometrical parameters on wear of hot forging die. *J. Mater. Res. Technol.* **2021**, *15*, 5221–5231. [[CrossRef](#)]
24. Bayoumi, L.S. Cold drawing of regular polygonal tubular sections from round tubes. *Int. J. Mech. Sci.* **2001**, *43*, 2541–2553. [[CrossRef](#)]
25. Fu, Z.Q. *Research on Continuous Roll Forming Process and the Computer Aided Design System of Shape Tube*; Yanshan University: Qinhuangdao, China, 2014. (In Chinese)
26. Du, F.S.; Xing, M.L.; Wang, H.J.; Fu, Y.T.; Pei, X.Y. Influence of pass parameters and pass configuration on rectangular tube forming. *J. Plast. Eng.* **2022**, *29*, 65–71. (In Chinese)
27. Chang, Y.; Wang, N.; Wang, B.T.; Li, X.D.; Wang, C.Y.; Zhao, K.M.; Dong, H. Prediction of bending springback of the medium-Mn steel considering elastic modulus attenuation. *J. Manuf. Process.* **2021**, *67*, 345–355. [[CrossRef](#)]
28. Lin, G.Y.; Feng, D.; Zheng, X.Y.; Yang, W.; Sun, L.P. Analysis of influence of extrusion times on total die wear based on Archard theory. *J. Cent. South Univ.* **2009**, *40*, 1245–1251. (In Chinese)
29. Luo, Z.; Sun, M.; Zhang, Z.; Lu, C.; Zhang, G.; Fan, X. Finite element analysis of circle-to-rectangle roll forming of thick-walled rectangular tubes with small rounded corners. *Int. J. Mater. Form.* **2022**, *15*, 73. [[CrossRef](#)]
30. Hong, S.; Lee, S.; Kim, N. A parametric study on forming length in roll forming. *J. Mater. Process Technol.* **2001**, *113*, 774–778. [[CrossRef](#)]

31. Ferreira, S.L.C.; Bruns, R.E.; Ferreira, H.S.; Matos, G.D.; David, J.M.; Brandão, G.C.; da Silva, E.G.P.; Portugal, L.A.; dos Reis, P.S.; Souza, A.S.; et al. Box-Behnken design: An alternative for the optimization of analytical methods. *Anal. Chim. Acta* **2007**, *597*, 179–186. [[CrossRef](#)]
32. Zhang, Z.K.; Li, X.B.; Zhao, Z.L.; Jiang, C.; Zhao, H. Process Optimization and Formation Analysis of Friction Plug Welding of 6082 Aluminum Alloy. *Metals* **2020**, *10*, 1454. [[CrossRef](#)]

**Disclaimer/Publisher's Note:** The statements, opinions and data contained in all publications are solely those of the individual author(s) and contributor(s) and not of MDPI and/or the editor(s). MDPI and/or the editor(s) disclaim responsibility for any injury to people or property resulting from any ideas, methods, instructions or products referred to in the content.